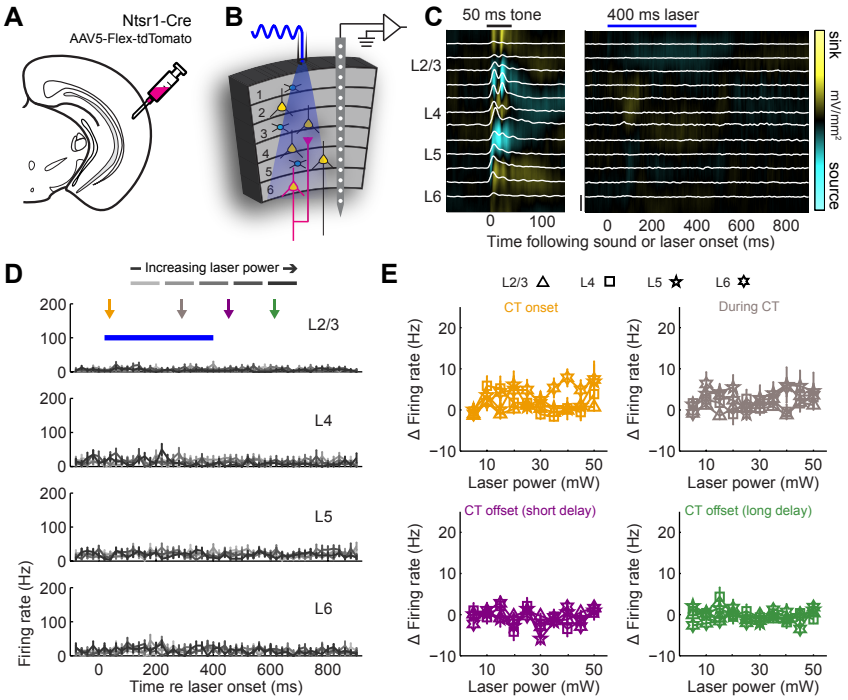

Fig. S1 (related to Figure 2) Laser does not evoke spiking activity from L6CT neurons expressing a control fluorophore. (A) A reporter fluorophore (tdTomato) was expressed in L6 CT neurons by injecting a Cre-dependent viral construct into A1 of Ntsr1-Cre mice. (B) Schematic of columnar recording and laser illumination. (C) Sound-evoked (left) and laser-evoked (right) laminar profiles of current source density (CSD) amplitude from a single A1 penetration in an awake mouse. Multiunit activity (MUA) at each location is represented by the superimposed white peristimulus time histograms (PSTH, scale bar = 100 spikes/s). (D) PSTHs represent the mean MUA in each layer for laser powers ranging from 5-50 mW at the tip of the fiber. Error bars represent 1 SEM. (E) Laser did not evoke spiking activity from any layer (mixed design ANOVA, $F(3) = 0.83$, $p = 0.48$) during any response period (mixed design ANOVA, $F(3) = 0.86$, $p = 0.46$). Error bars represent 1 SEM.

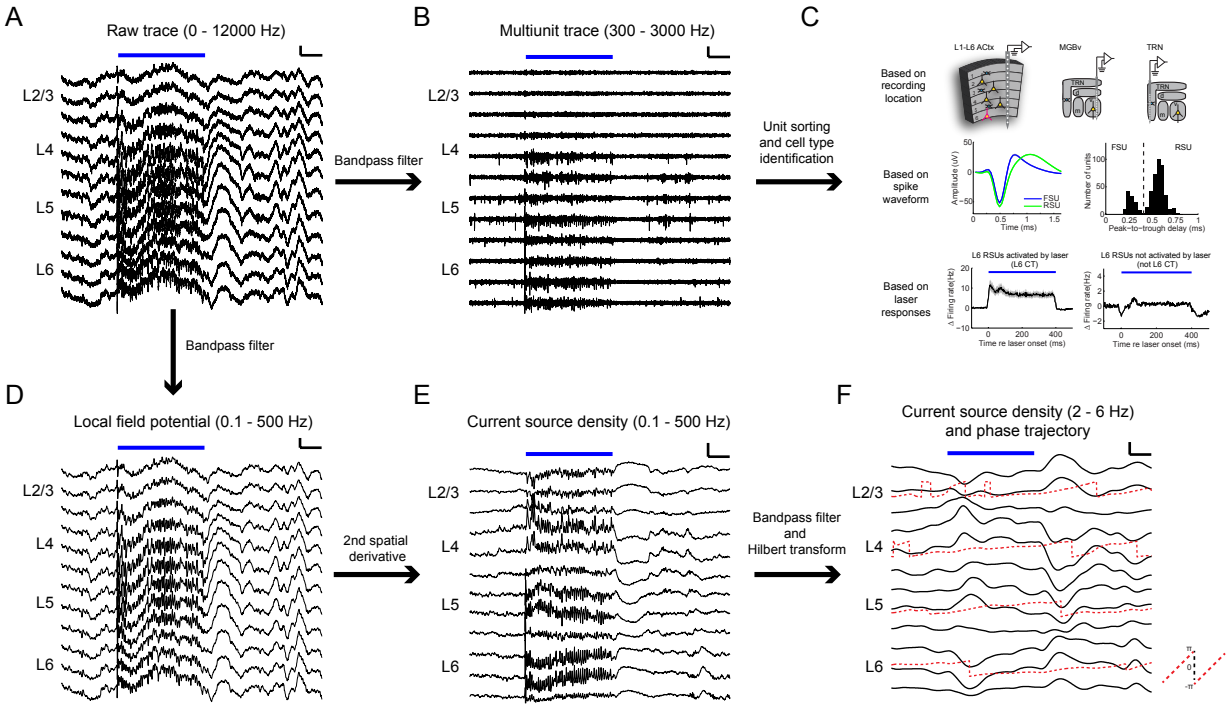

Fig. S2 (related to Figure 6 and 7) Signal processing and analysis of columnar recordings. (A) Unfiltered signal from a 16-channel silicon probe spanning all layers of A1 before, during and after L6 CT activation (scale bars: 100 ms, 250 μV). (B) The same data, bandpass filtered between 300 – 3000 Hz to reveal multiunit spiking. (scale bars: 100 ms, 100 μV). (C) Single units waveforms are isolated offline and classified as RS, FS or L6 CT according to waveform shape or sustained response to optogenetic stimulation. Units were classified as fast-spiking units (FSUs, peak-to-trough delay < 0.4 ms) and regular-spiking units (RSUs, peak-to-trough delay > 0.4 ms). Error bars on PSTH represent 1 SEM. (D) Bandpass filtering the raw data in (A) between 0.1 – 500 Hz reveals the local field potential. (scale bars: 100 ms, 250 μV). (E) The second spatial derivative of the local field potential provides the CSD signal across layers. (scale bars: 100 ms, 5 mV/mm^2). (F) CSD traces from (E) can be band-pass filtered between 2-6 Hz and the phase trajectories can be obtained using the Hilbert transform (scale bars: 100 ms, 5 mV/mm^2).

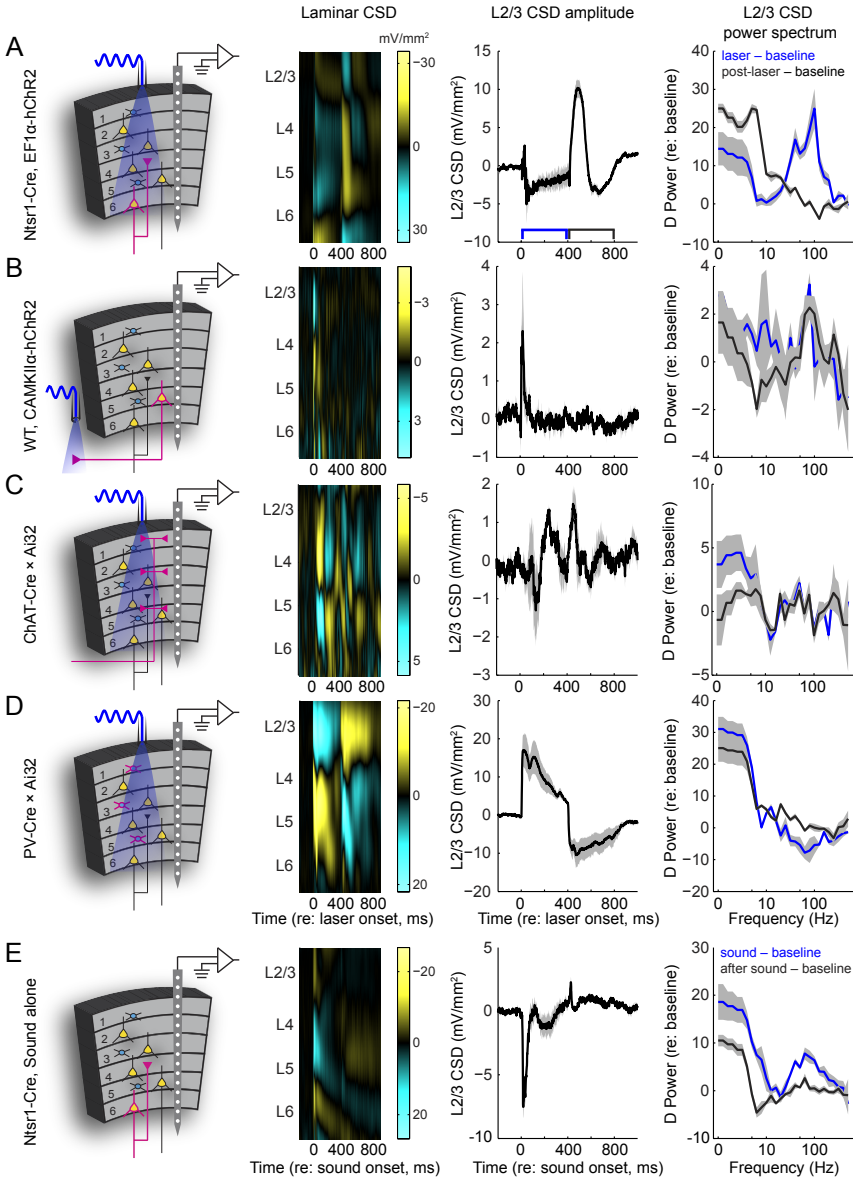

Fig. S3 (related to Figure 6) The laminar pattern of CSD changes evoked by activation of L6 CT neurons is not observed with optogenetic activation of other modulatory cell types. (A-D) Patterns of laser-evoked CSD amplitudes and frequency spectra when ChR2 is expressed in other cell types. First column, cartoon illustrating cell type-specific ChR2 expression. Second column, the laminar pattern of CSD sinks and sources for a representative recording in each condition. Third column, mean (±1 SEM) L2/3 CSD amplitude. Blue box denotes 400 ms laser period. Black box denotes 400 ms post-laser period. Fourth column, mean (±1 SEM) change in L2/3 frequency spectrum for the laser and post-laser periods relative to the baseline period (0-400 ms prior to laser onset). (A) L6 CT activation as per Fig. 6. (B) ChR2 is expressed in pyramidal neurons under the CamKIIa promoter. Optogenetic stimulation is restricted to L5 corticofugal neurons by stimulating axon terminals on the dorsal surface of the inferior colliculus, a midbrain structure. (C) Optogenetic activation is limited to cholinergic axons from the basal forebrain by crossing the ChAT-Cre mouse line (B6;129S6-Chattm2(cre)Lowl/J) with the Ai32 mouse line. (D) Optogenetic activation is limited to parvalbumin-expressing FS interneurons by crossing the PV-Cre mouse line with Ai32 mouse line [Ai32(RCL-ChR2(H134R)/EYFP)], in which ChR2 is expressed in cells with Cre recombinase. (E) Sound-evoked CSD changes in Ntsr1-Cre mice are provided for comparison with optogenetic activation. Note differences in Y-axis scaling between conditions. Also note that the distinctive pattern of high-gamma oscillations during activation followed by a 2-6 Hz large-amplitude post-laser offset CSD signal is only observed with L6 CT activation.

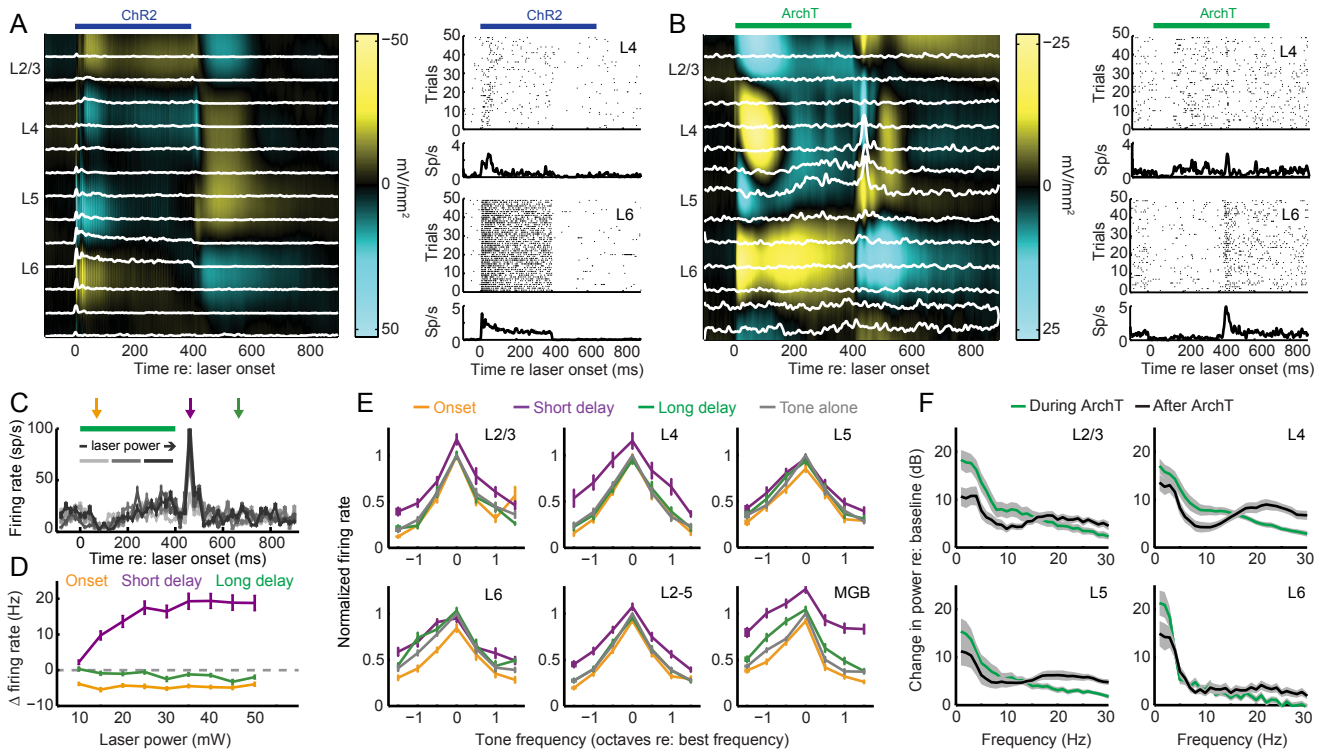

Fig. S4 (related to Figure 2, 5 and 6) Inactivation of L6CT neurons with the hyperpolarizing opsin, ArchT, induces the opposite effects of ChR2 in A1 and MGBv. (A) Left: Columnar CSD pattern in A1 induced by optogenetically activating L6CT neurons with ChR2. Right top: an example L4 unit responding to L6 CT activation. Right bottom: an example L6 CT unit responding to direct photoactivation. (B) Left: Columnar CSD pattern in A1 induced by optogenetically inactivating L6 CT neurons with ArchT. Right top: an example L4 unit firing rate changes before and after L6 CT inactivation. Right bottom: an example of firing rate changes in a L6 unit during inactivation, most likely from a L6 CT unit expressing ArchT. (C) Mean multiunit spiking PSTH from L2-5 relative induced by ArchT activation with laser powers ranging from 5–45 mW (light gray to black, respectively). Orange, purple and green arrows indicate the time epochs used to calculate firing rate changes at the onset, short delay and long delay periods, respectively. (D) Firing rate changes with ArchT inactivation are the opposite of activation with ChR2; relative to the pre-laser spontaneous firing, spiking is suppressed at laser onset, enhanced at a short delay (50 ms) following laser offset and weakly suppressed at a longer delay (150 ms) following laser offset. Dashed gray line indicates no change in firing rate. (E) Normalized tone-evoked firing rate relative to the unit's best frequency for the tone-alone condition (gray line) and the three laser conditions. Responses are enhanced during the short delay period following ArchT inactivation. (F) Changes in the low-frequency power spectrum (0-30 Hz) of the CSD signal for each layer of the A1 column relative to a baseline period for a time window during ArchT inactivation (green line) versus just after laser offset (black line). Error bars for all plots represent 1 SEM.